Journal of Applied Electrochemistry **30**: 293–302, 2000.

Characterization of doped tin dioxide anodes prepared by a sol–gel technique and their application in an SPE-reactor

J.H. GRIMM[1]*, D.G. BESSARABOV[1], U. SIMON[2] and R.D. SANDERSON[1]
[1]*Institute for Polymer Science, University of Stellenbosch, Matieland 7602, P/Bag X1, RSA*
[2]*Institute of Inorganic Chemistry, University of Essen, Germany*
*(*author for correspondence)*

Received 8 December 1998; accepted in revised form 31 March 1999

Key words: Electrochemical oxidation, sol–gel process, SPE, spin trapping

Abstract

Anodes for the electrocatalytic oxidation of organic pollutants in water have been prepared by depositing novel Sb-doped SnO_2 material on Ti supports by the sol–gel technique. Surface analysis of the anodes by nuclear microprobe and XPS-measurements confirmed the formation of a doped film on the substrate. Large scale porous titanium electrodes, up to 50 cm^2, have been coated with doped SnO_2 for a galvanostatic solid polymer electrolyte (SPE) application, resulting in very low voltage across the stack, even without adding supporting electrolytes to the water. Assessment of the cell performance was carried out using *N*,*N*-dimethyl-*p*-nitrosoaniline (RNO) as a spin trap for ·OH-radicals and phenol as a standard organic contaminant. Kinetic studies were done for the formation of the ·OH-radicals.

1. Introduction

The electrochemical destruction of waste in water has advantages in terms of cost and safety over other forms of waste water treatment. The process runs at high electrochemical efficiency and operates essentially under largely similar conditions for a wide variety of wastes [1]. One way in which the efficiency of electrochemical methods for waste water treatment can be increased is by supporting the system on solid polymer electrolytes (SPE). A specific area includes the improvement of electrocatalytic systems consisting of novel anodic materials such as SnO_2.

This paper deals with the study of Sb-doped SnO_2 anodes coupled with a perfluorinated cation-exchange membrane to build a system for the anodic oxidation of hazardous organics in water. As organic pollutants do not form sufficiently conductive electrolytes for the electrochemical treatment without the addition of supporting salts, an SPE reactor was designed. Since perfluorinated ion-exchange membranes such as Nafion® as an SPE are used to separate the anode and the cathode in the electrochemical oxidation process, no conductive liquid is required in the cell. An SPE system thus makes possible electroorganic reactions at an electrode on the surface of an ion exchange membrane without the need for addition of a supporting electrolyte [2]. This is feasible, because the fixed sulphonic acid groups in the polymer, similar to immobilized sulphuric acid, provide the ionic conductivity through proton mobility inside the membrane. Hydrogen ions are formed at the anode during oxidation and migrate through the cation-exchange membrane.

For the kinetic measurements of the reactions by which ·OH-radicals were formed at the anodes, PbO_2 based electrode material on Ebonex and the Ti/SnO_2/Sb_2O_5 anode material were compared. RNO was used as a spin trap for ·OH-radicals.

1.1. *Electrode material for electrocatalytic oxidation*

Sb-doped SnO_2 anodes are well-established as electrode materials for the oxidation of hazardous organics in water [3]. In this work the dip-coating sol–gel method [4] was selected over other established methods, such as chemical vapour deposition [5, 6], reactive sputtering [7] and spray pyrolysis [6, 8, 9] for the preparation of Sb-doped SnO_2-films on Ti substrates. This procedure has previously been used for the preparation of catalytically active membrane films [10, 11]. The method has major advantages [12]: Starting materials of high purity, ease of coating of large and complex-shaped substrates and low cost. Very high-quality SnO_2 layers with respect to structure and morphology can be obtained by the sol-gel dipping technique. Chemical modifications achieved readily by the addition of selected dopants to the sol, improve the conductivity of the film and enhance its catalytic activity. Moreover, the films provide a porous structure which enlarges the catalytic surface of the film. BET-surface areas of the powdered SnO_2/Sb_2O_5 mate-

rials in previous work, were in the range of 100 to 120 $m^2\ g^{-1}$ with a broad pore-size distribution and an average pore diameter of 0.80 nm. Further detailed information on the film characterisation has been given by Grimm et al. [13].

1.2. *Mechanism oxidation of organics in water and analytical methods for its verification*

Two different pathways for the anodic oxidation of undesired organics are described in the literature [3, 14, 15]: (i) electrochemical conversion, and (ii) electrochemical combustion. These are as follows.

(i) Electrochemical conversion transforms only the toxic nonbiocompatible pollutants into biocompatible organics, and biological treatment is still required after the electrochemical oxidation.
(ii) Electrochemical combustion yields CO_2 and water and no further purification is necessary.

Previous work [3, 14, 15] has indicated, that the accumulation of ·OH radicals favours the combustion reaction, while the introduction of oxygen into the electrode lattice results in conversion. Anodes with a high oxygen overpotential, such as Ti/SnO_2, Ti/PbO_2 and graphite-felt, favour electrochemical combustion [14–16]. The following mechanism for the formation of ·OH radicals on an oxide anode (MO_x) has been suggested by Comninellis [3]:

$$MO_x + H_2O \xrightarrow{k_{OH}} MO_x(\cdot OH) + H^+ + e^- \quad (1)$$

The destruction of organics proceeds by the reaction:

$$R + MO_x(\cdot OH)_z \xrightarrow{k_C} Z/2\ CO_2 + Z\ H^+ + Z\ e^- + MO_x \quad (2)$$

The ·OH radicals were detected by a method which is already well established in biology and biochemistry, that is spin-trapping with *N*,*N*-dimethyl-*p*-nitrosoaniline (RNO) [17]. RNO has a yellow coloured sensitive absorption band at 440 nm ($\varepsilon = 3.44 \times 10^4\ M^{-1}\ cm^{-1}$), and its bleaching upon acceptance of an e^- from the ·OH-radicals can easily be observed by means of u.v.–vis. spectrophotometry.

Thus, the rate of the bleaching reaction in the presence of *N*,*N*-dimethy-*p*-nitrosoaniline (RNO) is determined by k_{RNO}.

$$RNO + \cdot OH \xrightarrow{k_{RNO}} \text{spin-adduct} \quad (3)$$

Phenol was used as a standard contaminant during electrolysis. The catalytic activity of the film prepared in the work towards the oxidation of phenol has already been confirmed by cyclovoltammetry [13]. In the present work the decrease in the concentration of phenol was directly observed during galvanostatic electrolysis. The direct detection of the phenol concentration at 270 nm by means of u.v.–vis. spectrophotometry was interfered with heavy noise caused by the electrode process itself. To overcome that problem, an antipyrine dye was formed with 4-aminoantipyrine in the presence of hexacyanoferrate(III) with the maximum of absorbance at 510 nm. 4-aminoantipyrine exerts an electrophilic attack upon the para-position of the phenol to form a quinone structure [18].

To confirm these results the phenol index was additionally determined by a colorimetric method.

2. Experimental details

2.1. *Preparation of the SnO_2/Sb_2O_5 catalytic layers*

The doped SnO_2 solutions for the dip-coating were prepared from two alkoxides obtained directly from chlorides according to the method described by Chaleton [12]. A porous, circular titanium plate with a total area of 100 cm^2 was used as a substrate for the catalyst. It was placed in a clean chamber saturated with ethanol vapour. The sol was pipetted onto the substrate through a hole in the top of the chamber, coating both sides of the electrode. The substrate was then allowed to dry for 6 h, after which it was dried in air at 100 °C for 15 min in air. This coating procedure was carried out twice to close cracks and heal defects in the film. Calcination was then carried out in air by heating the substrate to 600 °C, at a rate of 1 °C min^{-1}. After the calcination process the electrode maintained its porous structure and was still permeable to water. For analysis of the film by XPS and microprobe, and for the kinetic studies with RNO, the samples were prepared by sol–gel dip-coating as previously described [13].

2.2. *Preparation of the PbO_2-based electrodes*

Plates of Ebonex [19, 20] were coated anodically for 30 min with PbO_2 in an acid solution of $Pb(NO_3)_2$ (c.d. 10 mA cm^{-2}, electrolyte: 0.4 M l^{-1} $Pb(NO_3)_2$, pH −0.3) [21].

2.3. *Surface analysis of the $Ti/SnO_2/Sb_2O_5$ anodes by microprobe and XPS*

The surface of the anode was investigated by X-ray spectroscopy at the National Acceleration Center of South Africa. The X-rays were activated by a proton beam. The XPS-analysis was carried out at the Institut für Physikalische und Elektrochemie II at the Heinrich-Heine-Universität Düsseldorf.

2.4. *Set-up of the electrochemical cell*

For the electrolysis the electrochemical cell consisted of a chamber with working and counter electrode, and was equipped with a fibre-optic spectrophotometer for u.v.–vis. analysis (Figure 1). The fibre-optic sensor is illustrated in Figure 2. This set-up was used for the kinetic

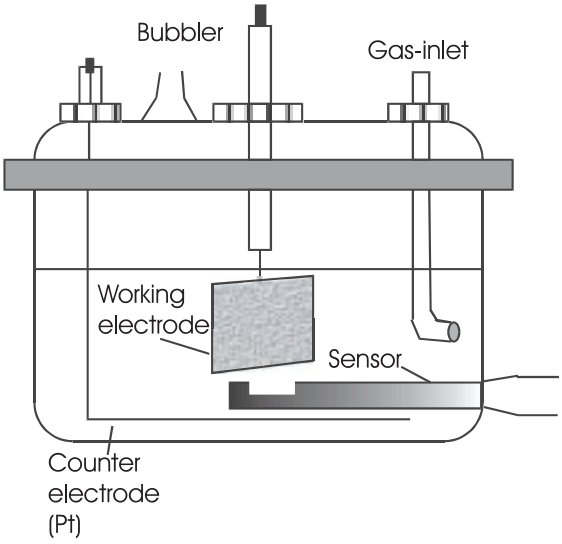

Fig. 1. Set-up for the electrochemical cell.

studies with RNO. The ·OH radical trapping was measured in a phosphate buffer (pH 7.0) containing 2×10^{-5} M/l RNO (ε = 34 200 M^{-1} cm^{-1} at 440 nm).

For the cyclic voltammetry we used an electrochemical measurement unit with a three-electrode cell. The reference electrode was based on a $Hg/HgSO_4/K_2SO_4$ (sat.) system, while all potentials given refer to RHE. The electrolyte consisted either of 1 M H_2SO_4 or 1 M H_2SO_4 and 5 mM phenol. The solution temperature was maintained at 25 °C. Prior to any measurement being made, nitrogen was bubbled through the electrolyte.

2.5. *Set-up of the SPE-reactor*

A porous Ti plate, coated with Pt by means of a magnetron sputtering on the surface and identical in shape to the anode, was used as a cathode. The two electrodes were mounted in the SPE reactor [21–23], sandwiching a perfluorinated Nafion®-like cation-exchange membrane in H^+-ionic form ('Plastpolymer', St. Petersburg, Russia), as shown in Figure 3. Membrane was prepared from copolymer of tetrafluoroethylene and perfluoro-3,6-dioxa-5-methyl-1-octene-8-sulfonyl fluoride. Thickness of the membrane was 230 μm, and equivalent weight was 1120.

The electrolyte (0.5l) was pumped through the reactor by a peristaltic pump, passing the anode and cathode chamber in series, while the cation-exchange membrane ensured the ionic migration between the two electrodes. The area of the electrodes was 100 cm^2.

2.6. *Online analysis of phenol during electrolysis in the SPE reactor*

The u.v.–vis. analysis was carried out with a Perkin Elmer Lamda 20 spectrophotometer attached to a fibre optics sensor placed inside the flow of the electrolyte (Figure 4).

The electrolyte for the phenol determination comprised: 0.1 M 4-aminoantipyrine, 2 mM $K_3[Fe(CN)_6]$, 1.3 mM NH_4Cl 0.03 M NH_4OH, 1.4 mM potassium sodium tartrate tetrahydrate and 0.1 mM phenol. The red absorption band was monitored at 510 nm.

2.7. *Phenol index*

The phenol index refers to the concentration in mg l^{-1} (M) of any phenolic compound. After a preliminary distillation of the phenol, the test samples were analysed by a direct colorimetric method. The analysis was carried out according to the German standard methods for the examination of water, waste water and sludge [24].

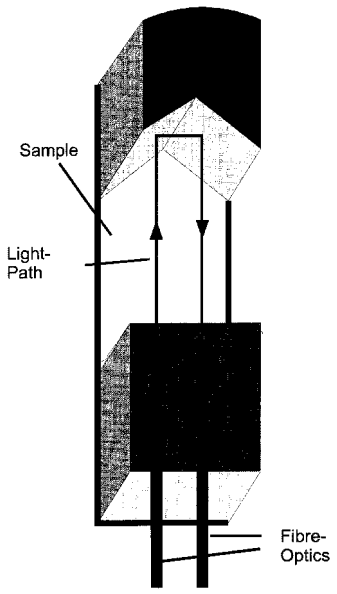

Fig. 2. Sensor for the RNO-determination for the fibre-optics spectrophotometer.

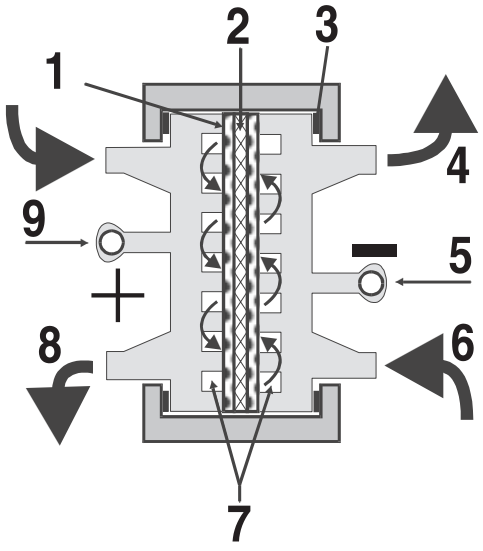

Fig. 3. SPE-reactor: (1) porous Ti, coated with SnO_2/Sb_2O_5, (2) Nafion® membrane, (3) isolators between electrodes and reactor, (4) outlet for water, (5) cathode side, (6) cathodic inlet for water, (7) distribution channels for cathode and anode, (8) anodic outlet, (9) anode side.

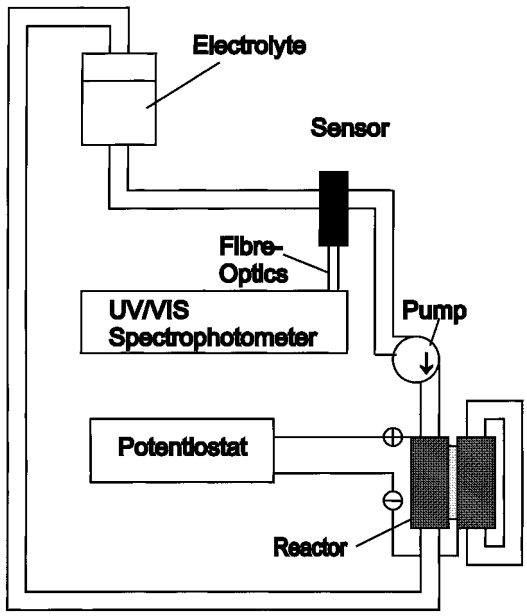

Fig. 4. Scheme for the online phenol analysis by the fibre-optics spectrophotometer.

2.8. *Electrochemical equipment*

All electrochemical measurements were carried out with a Solartron SI 1280B. Electrolysis was performed galvanostatically, with a current density of i = 20 mA cm^{-2}. Cyclic voltammetry was implemented using a three-electrode cell. The reference electrode was based on a $Hg/HgSO_4/K_2SO_4$ (sat.) system. The electrolyte consisted either of 1 M H_2SO_4 or 1 M H_2SO_4 and 5 mM phenol. The solution temperature was maintained at 25 °C. Prior to any measurement being made, nitrogen was bubbled through the electrolyte.

3. Results and discussion

3.1. *Surface analysis of the $Ti/SnO_2/Sb_2O_5$ by microprobe*

The surface of the electrodes with a doping level (Dp_{sol} ratio = $n_i/\Sigma n$) of 10% Sb was investigated by microprobe. The X-ray spectrum is shown in Figure 5. The ratio of Sn/Sb calculated by integration methods ranged from 9.9–12.8% for the Sb content, thus confirming that the dopant had been well mixed in the sol without detectable precipitation taking place.

Unfortunately, no information on the oxidation states of the elements could be obtained by this experimental method.

3.2. *Surface analysis by XPS*

To confirm the results from the microprobe analysis, further surface analysis was undertaken with XPS. The method provided additional information on the oxidation states of the coating. The entire spectrum is shown in Figure 6.

The catalytic layer of the electrode material was investigated. Information about the distribution of the elements and the oxidation state of the elements was obtained. The determination of the antimony was not straight forward, as its signal appears at the same binding energy as does the oxygen peak. The peak at 532 eV (Figure 7) had to be separated into an oxygen peak and an antimony peak. In our case this was done by making use of the relation between the pre-wave (Sb $3d_{5/2}$) at 532 eV and the wave at 541 eV (Sb $3d_{3/2}$) for antimony is fixed to be 1.44. This precondition was used for the fit in Figure 7.

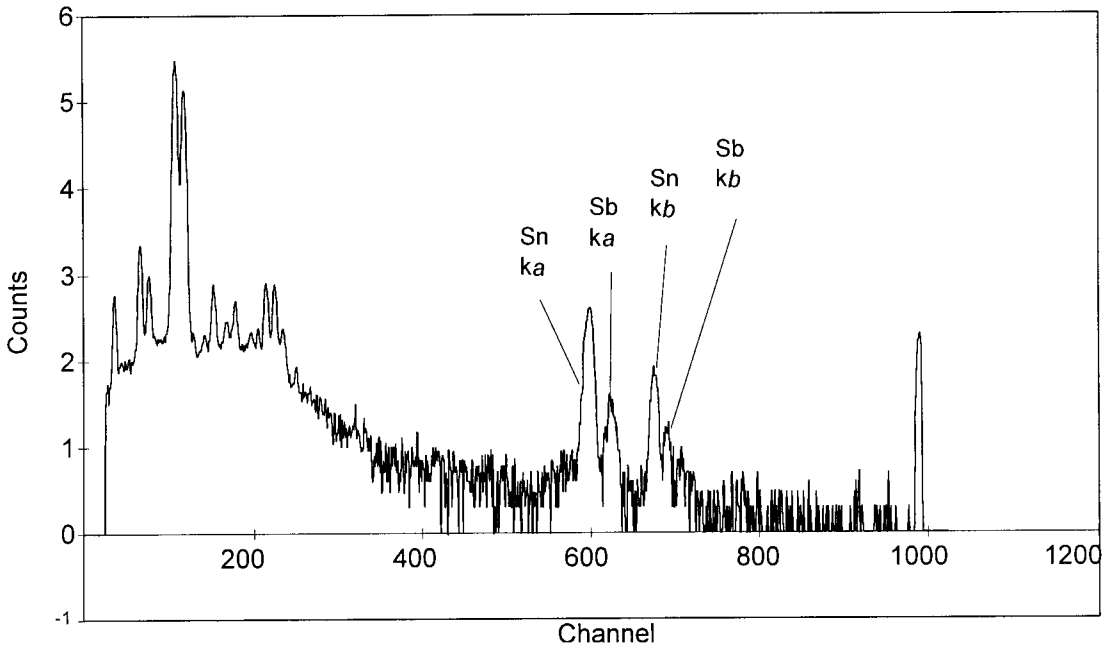

Fig. 5. X-ray spectrum of the surface of $Ti/SnO_2/Sb_2O_5$, the Sn and Sb peaks are indicated.

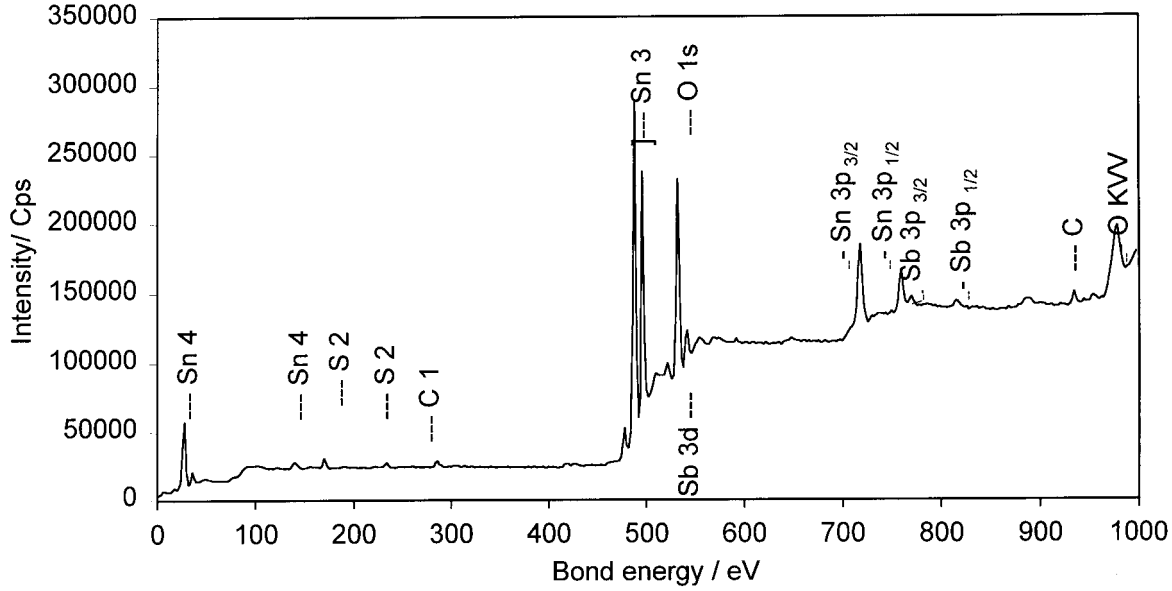

Fig. 6. XPS-spectrum of the $Ti/SnO_2/Sb_2O_5$ electrode.

The real areas of the peaks had to be calibrated according to the sensitivity of the instrumentation towards the particular elements. The atomic ratio between Sn and Sb was found to be 4:1. Since the doping level (Dp_{sol} ratio = $n_i/\Sigma n$) of Sb in the initial solution was 10%, part of the Sn must have precipitated out of the solution prior to the process of dip-coating.

The shift in the binding energy of the elements determined the oxidation number and Sn was found to have the oxidation number 4, while the shift for Sb indicated an oxidation number of 5, corresponding to the oxides SnO_2 and Sb_2O_5. The fact that traces of sulphur and copper were detected on the surface, is explained by the treatment of the samples before the XPS-analysis. The samples and sample-holders (Cu) were purified with 2 M H_2SO_4. Obviously, despite an attempt to remove them in an ultrasonic bath, small amounts of S and Cu had remained on the surface.

3.3. *Side anodic reaction of O_2 evolution*

Cyclic voltammetry was carried out to investigate the catalytic activity of the electrode material. The cyclic voltammic scans were carried out in 1 M sulfuric acid and 1 M sulfuric acid plus 5 mM phenol. Phenol is used

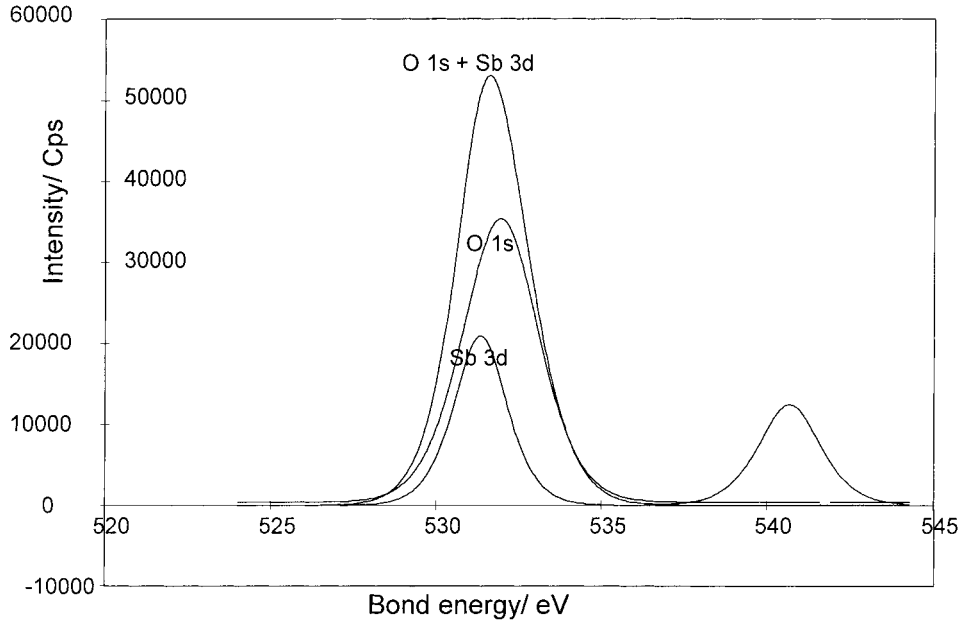

Fig. 7. Curve fitting for the separation of the oxygen and the antimony peak.

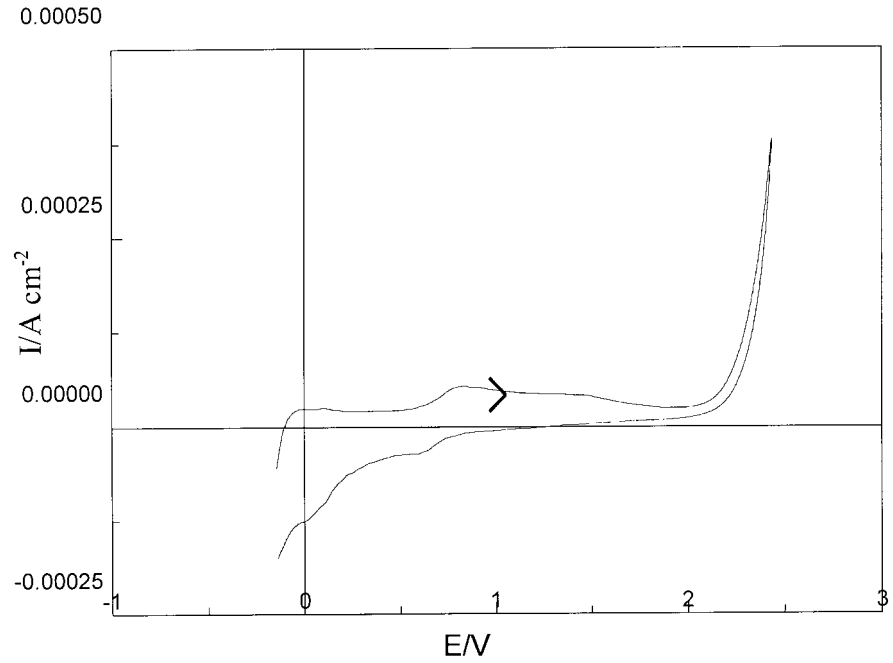

Fig. 8. Ti coated with SnO_2 + 10% Sb-content, electrolyte: 1 M H_2SO_4, v = 20 mV s^{-1} Potential against RHE.

as a standard contaminant. Prior to the measurement the electrode was scanned between the oxygen and the hydrogen potential until the cyclic voltammogram remained unchanged. The activity of the catalytic film towards combustion is indicated by the appearance of an additional peak or increase in the current in the anodic range after the addition of phenol to the electrolyte. Figure 8 shows the cyclic voltammogram in 1 M sulfuric acid. In Figure 9, after the addition of 5 mM of phenol, a new combustion peak appears. The peak is well separated from the oxygen evolution and thus, at its maximum of 1.5 V (NHE), it can be assumed that the combustion takes place without any side reactions. The oxygen evolution takes place at a high overpotential of 2.2 V vs NHE.

The same experiments on PbO_2 coated ebonex did not result in a separated combustion peak. There is still a high overpotential for the oxygen evolution, but upon the addition of phenol only an increase of the anodic current density is observed (Figures 10 and 11).

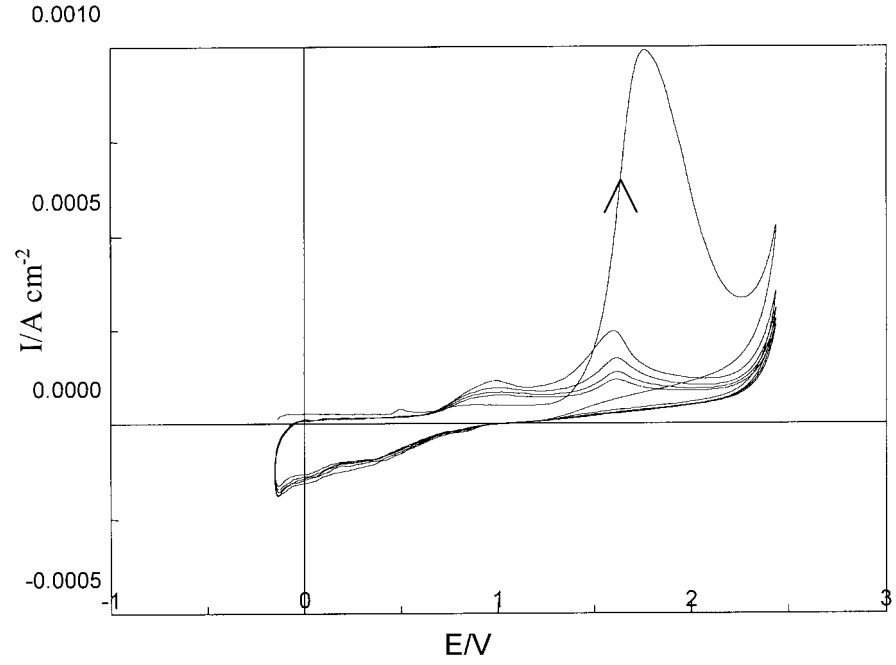

Fig. 9. Ti coated with SnO_2 + 10% Sb-content, electrolyte: 1 M H_2SO_4 + 5 mM phenol, v = 20 mV s^{-1}.

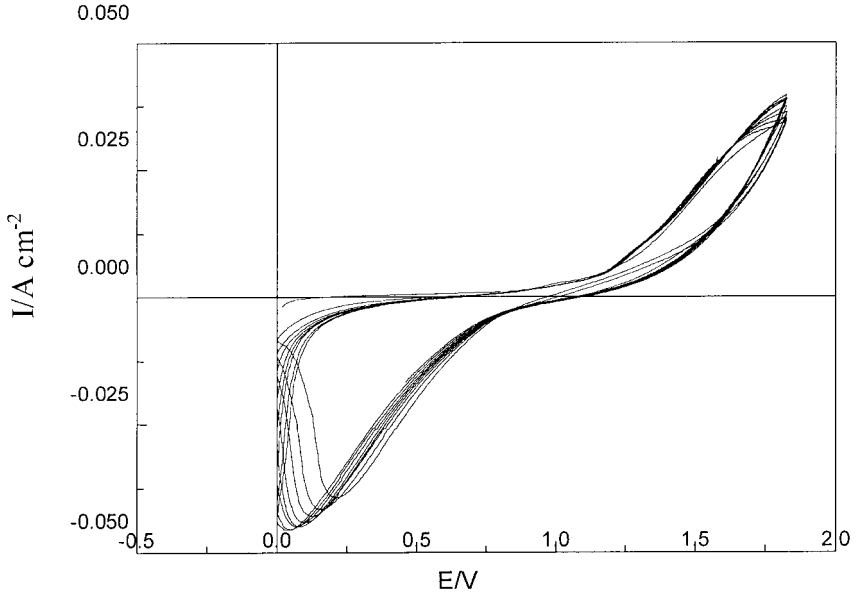

Fig. 10. Ebonex electrode, coated with PbO_2. Electrolyte: 1 M H_2SO_4, $v = 20$ mV s^{-1}.

3.4. *Spin-trapping of ·OH-radicals by N,N-dimethyl-p-nitrosoaniline (RNO)*

After the galvanostatic electrolysis on $Ti/SnO_2/Sb_2O_5$ and $Ebonex/PbO_2$ in a phosphate buffer solution with 2×10^{-5} M RNO, absorption curves were obtained for the bleaching of RNO (Figure 12):

The software program 'Mathcad 5.0 Plus' was used to determine the rate constants of Equation 1 or 3 and the order of the reaction. The program permitted the estimates of the reaction order and the rate constant the differential method being used to analyse the reaction data. Interpolation is carried out by spline function to generate equally spaced points.

Kinetic data obtained for PbO_2 -based electrodes are:

Reaction order: $a = 2.4$; specific velocity for a rate equation $dC/dt = k \times C^a$; $k = 0.134\,M^{-1}\,s^{-1}$; correlation: 0.967.

Correspondingly, the results for SnO_2-based material were:

$$a = 1.92;\ k = 0.155\ M^{-1}\,s^{-1};\ r = 0.959.$$

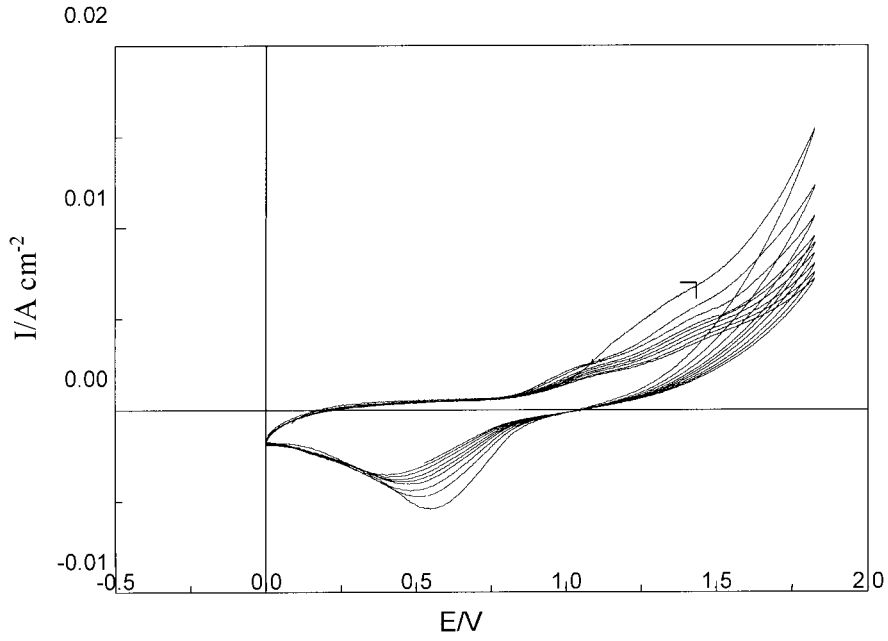

Fig. 11. Ebonex electrode, coated with PbO_2. Electrolyte: 1 M H_2SO_4 + 5 mM Phenol, $v = 20$ mV s^{-1}.

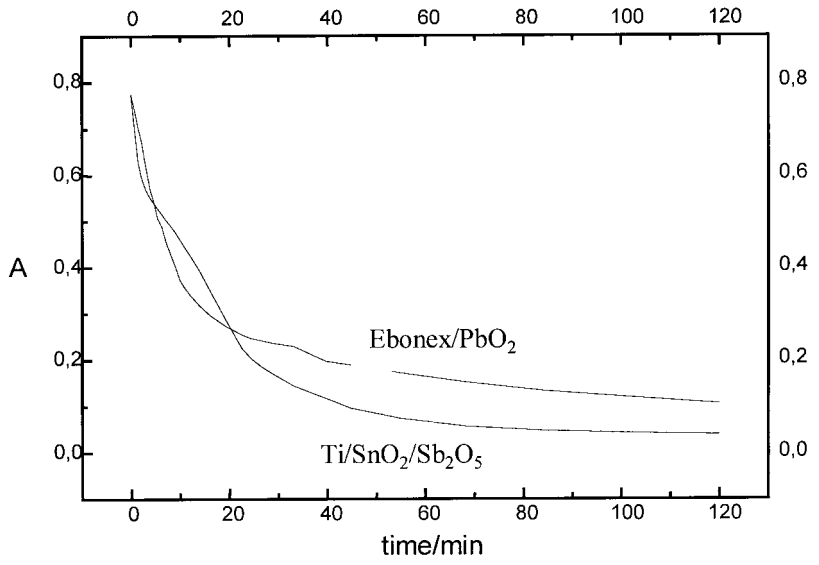

Fig. 12. Absorption against time during electrolysis for Ebonex/PbO_2 and Ti/SnO_2/Sb_2O_5. Current density: i = 20 mA cm^{-2}, electrolyte: phosphate buffer (pH 7) + 2×10^{-5} M RNO.

The reaction order of 2 is valid for both electrode materials.

3.5. *Determination of the phenol index*

Electrolyte (0.1 l), containing 1 g l^{-1} of phenol, was pumped through the SPE reactor during electrolysis at a current density of 20 mA cm^{-2} for 1200 min. Analysis was carried out every 15, 30, 60, 120, 240, 480, 720 and 1200 min. After a preliminary distillation and extraction with chloroform, the test samples were analysed [23].

The concentration of the phenol decreased from 1 to 0.22 g l^{-1} after 960 min of electrolysis. Further electrolysis could not significantly decrease that concentration. Figure 13 shows the decrease in phenol concentration versus time.

The current efficiency was calculated under the assumption that 28 electrons are required for the complete oxidation of one molecule of phenol. With the phenol concentration decreasing, the current efficiency is also going down. After 15 min of electrolysis the current efficiency reaches 22.3%, decreasing to still 7% after 120 min and finally only achieving 2% after 1200 min of electrolysis, as shown in Figure 14.

3.6. *Online phenol analysis with 4-aminoantipyrine by fibre-optics*

For the online determination of phenol, 0.1 mM of phenol was mixed with 0.1 M 4-aminoantipyrine, 2 mM $K_3[Fe(CN)_6]$, 1.3 mM NH_4Cl 0.03 M NH_4OH and 1.4 mM potassium sodium tartrate tetrahydrate to form 0.5 l of the coloured antipyrine dye which was pumped through the reactor at a current density of 20 mA cm^{-2}. The concentration of the phenol was determined by the fibre-optics spectrophotometer at a wavelength of 510 nm. Figure 15 illustrates the decrease of the phenol concentration, against time during electrolysis.

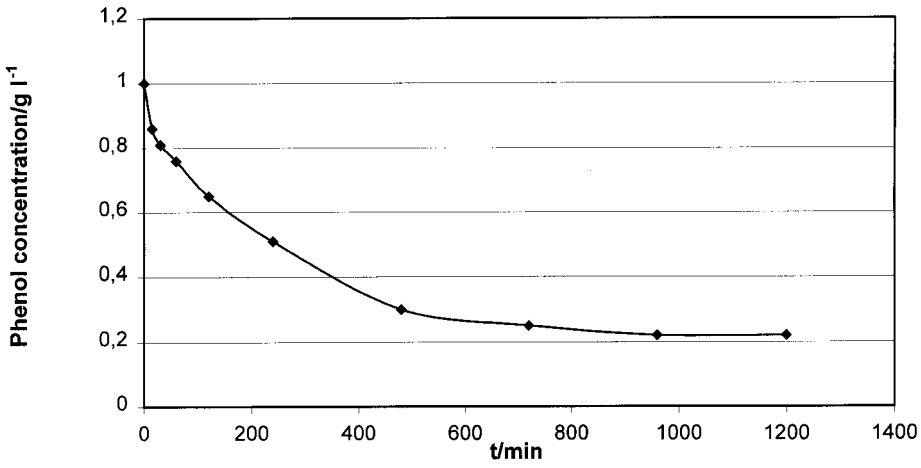

Fig. 13. Phenol concentration (g l^{-1}) against electrolysis time in the SPE-reactor, current density: 20 mA cm^{-2}.

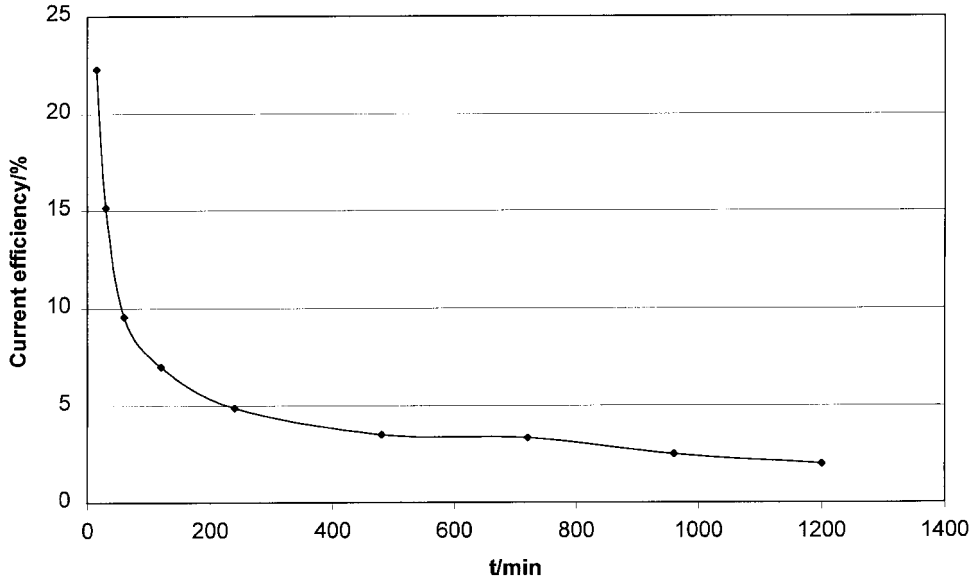

Fig. 14. Current efficiency against time of electrolysis.

By using the perfluorinated cation-exchange membrane inside the reactor the voltage drops from 17 to 3.35 V.

The concentration drop was not as rapid as shown for the accurate determination in Section 3.4, but seems to resemble the situation described there quite well. This indicated that the destruction of the quinone structure formed between phenol and 4-aminoantipyrine, was much more stable than the phenol itself, and that more accurate direct assessment of the phenol combustion process was not possible. Part of the inaccuracy can also be attributed to mass transport limitation to the fibre-optic sensor.

3.7. *Discussion*

A novel electrode material was prepared and tested in an SPE-reactor. XPS and microprobe analysis confirmed the incorporation of Sb_2O_5 into the SnO_2 film as a dopant, although the results indicated that some of the Sn-salts did not remain completely dissolved in the solution. The phenol concentration could be reduced considerably during electrolysis.

The pathway of the electrochemical combustion was confirmed by the detection of ·OH-radicals by spin trapping by RNO during electrolysis. The reaction order of the overall reaction is 2. Unfortunately, this reaction order could satisfy either of the second order equations, Equation 1 or Equation 3, two successive reactions, so that one of them must be predominately rate-determining, meaning that either $k_{OH} \gg k_{RNO}$ or $k_{OH} \ll k_{RNO}$. Equation 3 was independent of the electrode material, because the radical reacted directly with the RNO. The difference in the rate constants could thus be explained only by the initial reaction during which the radicals are formed. Consequently, Equation 1 must be the rate

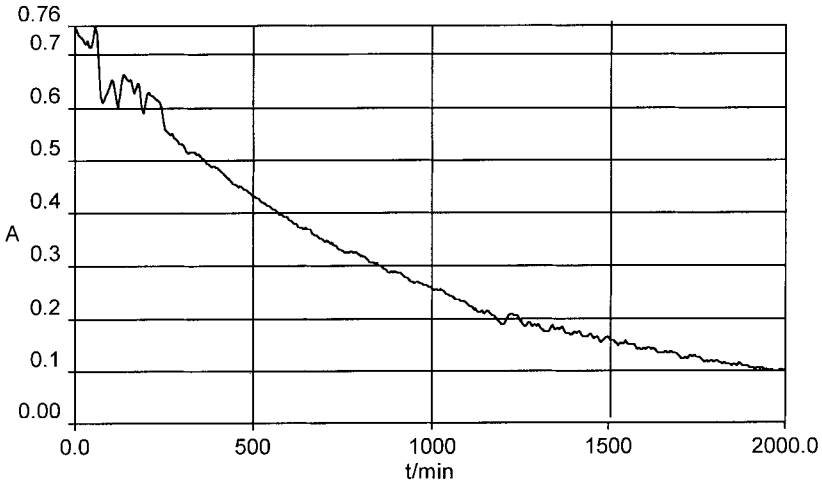

Fig. 15. Phenol concentration with 0.01 g l^{-1} as initial concentration. Complexing agent: 4-aminoantipyrine, Online-detection at 510 nm, electrolysis in SPE-reactor, i = 20 mA cm^{-2}.

determining step of the whole reaction, and the calculated data valid for that particular step. This was in accordance with the literature [3], where the rate constant for Equation 3 of $k_{RNO} = 1.2 \times 10^{10}\ M^{-1}\ s^{-1}$ is reported, a far higher value than calculated here. Therefore, the overall reaction was assumed to be second order, with $k_{RNO} \gg k_{OH}$ and the first equation is the rate-determining step.

The absorption curves in Figure 3 also indicate that ·OH radical production is kinetically increased by the SnO_2-based material, what led also to a lower final concentration of RNO.

The reactor design, facilitating the Nafion membrane to separate anode and cathode proved to be very effective, delivering very low voltage.

Direct phenol determination by fibre-optics was possible only with loss of accuracy, because the quinone structure formed between the 4-aminoantipyrine and the phenol, seems to be more stable to electrocatalytic attack than the phenol alone was. Furthermore, mass transportation limits to the fibre-optics sensor must be considered.

In an SPE-application sol–gel SnO_2-based electrodes were a very powerful electrochemical tool for the electrochemical water purification of organic pollutants.

Upgrading of the system is easy to conceive, as any number of stacks of the described reactor design can be mounted together as required. The losses in current efficiency can be explained through side reactions such as oxygen evolutoltion. The cyclovoltammograms, however, show a clearly separated, sharp phenol peak. Thus further study will focus on finding the suitable current density for a variety of phenol concentrations, so that at any point, side reactions can be suppressed to a minimum.

Acknowledgements

We gratefully acknowledge the assistance of Michael Hirschfeld at the Institut für Physikalische und Elektrochemie, Heinrich-Heine-Universität Düsseldorf for the XPS-analysis. We also thank Dr Prozcetzky from the National Acceleration Center, South Africa, for the surface analysis by microprobe.

References

1. J. Grimm, D.G. Bessarabov and R.D. Sanderson, *Desalination* **115** (1998) 285.
2. Y.-L. Chen and T.-C. Chou, *J. Electroanal. Chem.* **360** (1993) 247.
3. C. Comninellis, *Electrochimi. Acta* **39** (1994) 1857.
4. N.J. Arfsten, *J. Non-Cryst. Solids* **63** (1984) 243.
5. M.R. Kadam, N. Vittal, R.N. Karekar and R.C. Aiyer, *Thin Solid Films* **187** (1990) 199.
6. L.I. Popova, M.G. Michailov, V.K. Gueorguiev and A. Shopov, *Thin Solid Films* **186** (1990) 107.
7. A. Czapla, E. Kusior and M. Bucko, *Thin Solid Films* **182** (1989) 15.
8. U.R. Chaudhuri, K. Ramkumar and M. Satyan, *J. Phys. D.* **23** (1990) 994.
9. T. Karlsson, A. Smith and J.F. Baumard, *Thin Solid Films* **208** (1992).
10. W.F. Maier, I.C. Tilgner, M. Wiedorn, H.C. Ko, A. Ziehfreund and R. Sell, *Adv. Mater.* **10** (1993) 730.
11. W.F. Maier, C.H. Ko, *Catal. Today* **25** (1995) 429.
12. C. Lange, B. Tesche, S. Storck and W.F. Maier, *J. Catal.*, in print
13. J. Grimm, D. Bessarabov, W. Maier, S. Storck and R.D. Sanderson, *Desalination* **115** (1998) 295.
14. C. Comninellis and A. De Battisti, *J. Chim. Phys.* **93** (1996) 673.
15. O. Simond, V. Schaller and C. Comninellis, *Electrochim. Acta* **42** (1997) 2009.
16. C. Comninellis and E. Plattner, *Chimia* **42** (1988) 250.
17. D. Wabner and C. Grambow, *J. Electroanal. Chem.* **195** (1985) 95.
18. J.K. Spiker, D.L.Crawford and E.C. Thiel, *Appl, Microbiol. Biotechnol.* **37** (1992) 518.
19. S.Y. Park, S.I. Mho, E.O. Chi, Y.U. Kwon and H.L. Park, *Thin Solid Films* **258** (1995) 5.
20. J.E. Graves, D. Pletcher, R.L. Clarke and F.C. Walsh, *J. Appl. Electrochem.* **22** (1992) 200.
21. D.G. Bessarabov and J.Grimm, Papers of the Water Institute of South Africa – Biennial conference, vol. 1, Cape Town (4–7 May 1998), p. 4.
22. D.G. Bessarabov, R.D. Sanderson, Y.M. Popkov, V.V. Valuev and S.F. Timashev, *Ind. Eng. Chem. Res.* **36** (1997) 2487.
23. O.J. Murphy et al., *Wat. Res.* **26**(4) (1992) 443.
24. Deutsche Norm, Deutsche Einheitsverfahren zur Wasser-, Abwasser- und Schlammuntersuchung, DIN 38 409 Teil 16, Bestimmung des Phenol-Index (H16).